Phase boundaries and the Widom line from the Ruppeiner geometry of fluids

Karlo de Leon [*]
Graduate School of Arts and Science, New York University, New York, New York 10003, USA

Ian Vega
National Institute of Physics, University of the Philippines, Diliman, Quezon City 1101, Philippines

(Received 12 June 2022; accepted 27 September 2022; published 17 November 2022)

The Ruppeiner geometry has been shown to provide novel ways for constructing the phase boundaries and the Widom line of certain fluids. This paper examines the applicability of these geometric constructions to more general fluids. We develop a general equation-of-state expansion for fluids near a critical point that mainly assumes analyticity with respect to the number density. Based on this general parametrization of fluids, we prove the equivalence of the Ruppeiner geometric construction and the standard Maxwell construction of phase boundaries near the critical point. In contrast, we find that the usual prescription based on the Ruppeiner geometry for the Widom line does not produce the expected Widom line for arbitrary cases of our general fluid equation of state. This usual prescription relies on the Ruppeiner metric induced on a particular hypersurface of the thermodynamic manifold. We show that by choosing a different hypersurface, which we call the Ruppeiner-N surface, and using its associated induced metric, the Ruppeiner construction generates the entire Widom line of the van der Waals fluid exactly, even away from the critical point. Interestingly, this alternative hypersurface yields another benefit. It improves the classification scheme originally proposed by Diósi *et al.* for partitioning the van der Waals state space into its different phases using geodesics of a thermodynamic metric. We argue that, whereas the original Diósi boundaries did not correspond to any clear thermodynamic lines, the corresponding boundaries based on the Ruppeiner-N metric become sensitive to the presence of the van der Waals Widom line and provide the correct classification of all van der Waals states. These results suggest that the Ruppeiner-N surface may be the more appropriate hypersurface to use when studying phase diagrams with thermodynamic geometry.

DOI: 10.1103/PhysRevE.106.054141

I. INTRODUCTION

Geometric ideas in thermodynamics trace a long illustrious history [1–7]. In one sense, this is quite natural. Already, one can see intimations of geometry in determining the stability of thermodynamic states. Thermodynamic stability demands the convexity or concavity of fundamental-relation surfaces. An equilibrium state on the entropy hypersurface $S = S(X^i)$, where X^i are natural extensive variables for entropy, is stable when the surface at that point is concave [8]. The concavity of the entropy is encoded in its stability matrix, or its Hessian, D^2S. This significance of a (proto-)geometric property, the concavity, in the thermodynamics of systems has motivated explorations of other geometric properties of thermodynamics that have broad physical significance. It remains a fascinating question just how much of the thermodynamics can be viewed from the lens of geometry and what applications are enabled by such a geometric viewpoint.

One complication toward this goal is that there is no unique or natural metric for thermodynamics [9,10]. Instead, different metrics for thermodynamic spaces have been proposed in the literature, depending on the application and on what aspects of thermodynamics one wishes to highlight. The earliest proposed metric appears to be that of Weinhold [6], who defined it as the Hessian of the internal energy D^2E. Weinhold showed that the laws of thermodynamics can be restated as mathematical statements requiring the Weinhold metric to be Riemannian. Closely related to this, though coming from an entirely different motivation, is the Ruppeiner metric [7]. This metric is instead the negative Hessian of the entropy $-D^2S$ whose interpretation is rooted in thermodynamic fluctuation theory [11]. These two metrics were later shown [12] to be conformal to each other through a factor of temperature: $D^2E = T(-D^2S)$.

Since the introduction of the Ruppeiner metric [7], a substantial body of work [11,13–15] has been directed toward firming up its theoretical groundwork as well as developing its potential uses. The Ruppeiner metric has found many important applications in thermal physics, such as in fluctuation theory [14], finite-time thermodynamics [16–18], phase transitions [15,19–26], and even black hole thermodynamics [25–27], among others.

Given a metric, the immediate objects of interest are its geodesics and curvature. Much of the work [15–27] on the Ruppeiner metric is anchored on these two geometric objects,

[*]Majority of the work done at National Institute of Physics, University of the Philippines, Diliman, Quezon City, 1101, Philippines; knd8618@nyu.edu

though most papers tend to deal with either one or the other. In the present work, we shall explore both. In particular, we shall reexamine the use of geodesics and the curvature of the Ruppeiner geometry in the construction of fluid phase diagrams.

Geodesics in thermodynamic geometry admit different physical interpretations. Some possibilities include the following: (1) the most probable path that fluctuations can drive the system from A to B, which derives from fluctuation theory [7,14], (2) the path of minimum number of distinguishable fluctuations between A and B [28], or (3) the path of least dissipation in a finite-time process [16–18].

In a pioneering study, Diósi *et al.* [29] proposed to classify the different phases of the van der Waals fluid using geodesics of the Ruppeiner geometry. The motivation for this was to provide a coordinate-independent (i.e., geometric) definition for the fluid phases. In the standard thermodynamic analysis, the phases of two distinct states below the critical point are operationally defined in terms of isotherms and isobars. This is tantamount to singling out a special coordinate system on the thermodynamic state space, which would be anathema to a geometric treatment of thermodynamics. The use of geodesics for classifying the thermodynamic phases frees it from this apparent coordinate dependence. This was achieved by Diósi *et al.* to some degree. However, as we shall see below, their prescription suffers from a key weakness: The region boundaries of their geodesics tend not to correspond to any physically meaningful thermodynamic line. In this paper, we show that in using a different submanifold of the Ruppeiner metric space, geodesics-based boundaries shows a clearer physical connection. Geodesics in this submanifold become sensitive to the presence of the Widom line, a thermodynamic line considered by many [30–32] to be the continuation of the coexistence curve on the supercritical region of a fluid.

The usual Ruppeiner metric is computed with the volume set constant. As explained by Ruppeiner [11], a constant volume (V) analysis allows for ready interpretation of quantities, such as the Ricci curvature being correlated with the correlation length. This translates to limiting the analysis on the constant-V hyperplane of the thermodynamic manifold, hence we call this submanifold the *Ruppeiner-V surface*. In the alternative method we propose, we allow the volume to change and keep the number of particles N constant instead, thus working on a constant-N hyperplane we call the *Ruppeiner-N surface*. We show here how the Ruppeiner-N surface can provide better results than the conventional Ruppeiner-V surface.

As a short digression, we clarify the definition of the Widom line. The term "Widom line" is used rather loosely by different authors. Originally, it was defined as the locus of points around a critical point that maximize the correlation length [30,32]. Whether this maximum is taken along isobars [19,22,32,33] or isotherms [30,31,34] tends to be ambiguous in the literature. Since correlation lengths are challenging to measure or compute, the Widom line is often indirectly obtained through the maxima of thermodynamic response functions, such as the isobaric heat capacity, isothermal compressibility, or the thermal expansion coefficient [20,30]. These response functions scale as powers of the correlation length near the critical point, and so their maxima should all asymptote to the Widom line as they approach the critical point. While this method is disputed by some authors [20,33], it has become the established technique for obtaining the Widom line, with the isobaric heat capacity most often used as the response function for tracking the correlation length [19,33,35]. Due to this, some authors [35] refer to the Widom line directly as the locus of points that maximize the isobaric heat capacity. In order to differentiate these two distinct notions of the Widom line, we refer to the correlation-length-based curve as the *statistical* Widom line (since the correlation length is a statistical quantity) and the heat-capacity-based curve as the *thermodynamic* Widom line (in the same spirit, since the heat capacity is a thermodynamic quantity). Furthermore, we may add the qualifiers "isobar" and "isotherm" to clarify along which paths the maxima are taken.

Distinctions aside, the Widom line gained the attention of the scientific community when various systems were observed to undergo abrupt changes in its properties when crossing the purported line [32,33,36,37]. Some supercritical fluids have been shown to possess liquidlike properties on one side of the line and gaslike properties on the other [31]. Given the importance of the Widom line, it is thus desirable for a thermodynamic geometry to be sensitive to it, and in this paper we show that this is achieved with geodesics of the Ruppeiner-N metric and not the usual Ruppeiner-V metric.

Complementing the geodesic structure of thermodynamic geometry is its curvature, which has also been proposed to hold thermodynamic significance. Many investigations of the Ricci scalar curvature [14] for different thermodynamic systems indicate its sign to reveal the nature of the dominant intermolecular forces in a system. For example, the curvature of a simple ideal gas vanishes everywhere, whereas the Fermi and boson gas have positive and negative curvatures, respectively [14]. Further examples are reviewed in Ref. [14]. The physical meaning of the magnitude of the Ricci scalar remains topical in thermodynamic geometry. Ruppeiner [7,14,15,19] has hypothesized that the magnitude of the Ricci scalar is proportional to the correlation volume near the critical point

$$R \propto \xi^3. \tag{1}$$

This relation has been shown to hold for many systems [7,38–46], though it has not yet been proven to be generally true. Quite notably, the Ricci scalar and the correlation length both diverge at the critical point, and both are found to have the same critical exponent [15].

Combined with Widom's argument that the correlation lengths of coexistent states are equal [47], Ruppeiner's conjecture implies that the Ricci curvature of coexistent states should also be equal. This enables a geometric construction of phase boundaries using the Ricci curvature. That is, in contrast to the standard approach in which we equate the Gibbs free energy of two coexistent states to find the phase boundary, in a geometry-based construction we equate their Ricci curvatures instead [19]. We call the boundary generated using standard methods the *Maxwell* phase boundary (from Maxwell's equal area law), and the Ricci-based boundary the *Ricci* phase boundary. This alternative method of obtaining the phase boundary is sometimes referred to as the *R-crossing method*. It has been applied to many different systems [19–21,23–26]. In each of these specific cases, excellent agreement is found between the two phase boundaries *near the critical point*. In

this work, we wish to check if this agreement holds for a wide class of fluids.

To achieve this, we construct a general parametrized expansion of fluid equations of state (EoSs) near the critical point and then calculate the associated thermodynamic metrics and their curvature. We then use the resulting parametrized EoS to assess the general validity of the *R*-crossing method. Indeed, we provide an explicit proof that the Maxwell and Ricci phase boundaries must agree near the critical point for our broad family of fluids.

The Ricci scalar has been used not only for constructing phase boundaries but also for the (statistical) Widom line [19,20]. This logically follows from Ruppeiner's hypothesis in Eq. (1) and the notion of the statistical Widom line as the locus of local correlation length maxima: If the correlation length is maximized, then so should the Ricci scalar. We shall call the Widom line generated from the Ricci scalar the *Ricci-Widom line*. Using the Ruppeiner-*V* metric, May and Mausbach [20] calculated the Ricci-Widom line of the van der Waals fluid and compared it to its thermodynamic Widom line and found the curves to have equal slopes at the critical point. In this paper, we show that if the Ruppeiner-*N* metric was used instead, the agreement is much better: The van der Waals thermodynamic Widom line and Ricci-Widom line are exactly the same, even when far from the critical point.

Taken together, all these results suggest that the Ruppeiner-*N* metric, through its geodesics and curvature, may be the more appropriate metric to use when constructing fluid phase diagrams with thermodynamic geometry.

The rest of the paper is organized as follows. In Sec. II, we review the fundamentals of the Ruppeiner metric. We then proceed to Sec. III to discuss the application of the Ruppeiner-*N* metric in characterizing the phases of the van der Waals fluid. We also give a review to the study of Diósi *et al.* [29] regarding this partitioning scheme. In Sec. IV, we present the parametrized fluid EoS expansion we designed specifically for Ruppeiner metric applications. These results are used in Sec. V where we investigate the relation of the Ruppeiner curvature to a system's phase boundary and Widom line. Finally, we conclude the paper in Sec. VI.

II. RUPPEINER METRIC

A. Geometry from thermodynamic fluctuation theory

The Ruppeiner geometry naturally emerges from thermodynamic fluctuation theory [11]. The latter is what lends a physical interpretation to the concept of length in a thermodynamic space. For completeness, we shall briefly review this here.

Consider a system in contact with its environment and whose equilibrium macrostate is at A_0. With the assumption of equal microstate probabilities, the probability of the system to be at a macrostate A must be proportional to the number of microstates of A:

$$P_A \propto \Omega_A. \tag{2}$$

By inverting Boltzmann's equation $S = k \ln \Omega$, we can write this probability in terms of thermodynamic quantities:

$$P_A \propto \exp\left(S_A^U/k\right), \tag{3}$$

where S_A^U is the entropy of the universe when the system is at state A and k is the Boltzmann constant. Equation (3) is a well-known relation used by Einstein in fluctuation theory [48]. To incorporate the phenomenon of fluctuation in our analysis, we expand the entropy about the equilibrium state A_0:

$$S^U = \sum_{n=0}^{\infty} \frac{1}{n!}\left[(d\mathbf{X}\cdot\nabla)^n_{A_0} S + (d\mathbf{X}'\cdot\nabla')^n_{A_0} S'\right], \tag{4}$$

where the X^μ components of $\mathbf{X}$ are the natural extensive variables of the entropy. Unprimed variables denote system quantities while primed variables denote environment quantities. Because A_0 is the equilibrium state, the $n = 1$ terms of Eq. (4) are all zero. Up to the leading nonvanishing order, the entropy of the universe is then

$$S^U = S^U_{A_0} + \left[\tfrac{1}{2}(\mathbf{dX}\cdot\nabla)^2_{A_0} S + \tfrac{1}{2}(\mathbf{dX}'\cdot\nabla')^2_{A_0} S'\right]. \tag{5}$$

The Hessians of S and S' already appear in the second and third terms of Eq. (5), respectively. To set the scale of the system, we keep one extensive variable constant. Let this scale variable be X^{sc}. This also fixes the corresponding environment extensive variable X'^{sc}. We then take the densities of the extensive variables with respect to scale variables, i.e., $x^\mu := X^\mu/X^{\mathrm{sc}}$ and $x'^\mu := X'^\mu/X'^{\mathrm{sc}}$. Because extensive quantities are conserved for a closed system such as the universe, $dx'^\mu = -\epsilon\, dx^\mu$, where $\epsilon = X^{\mathrm{sc}}/X'^{\mathrm{sc}}$. The last term in Eq. (5) is of the order ϵ^2. Assuming that the environment is very large compared to the system, in the sense that $X^{\mathrm{sc}} \ll X'^{\mathrm{sc}}$ ($\epsilon \ll 1$), we only keep that lowest-order term in ϵ, which is the zeroth order. Finally, dropping the last term of Eq. (5) and plugging this expression of the entropy to Eq. (3) we get

$$P_A = C \exp\left[-\frac{1}{2k}\left(-\frac{\partial^2 S}{\partial X^\alpha \partial X^\beta}\right)_{A_0} \delta X_A^\alpha \delta X_A^\beta\right], \tag{6}$$

where C is the normalization constant, and $\delta X_A^\alpha := X_A^\alpha - X_{A_0}^\alpha$. We are using Einstein's summation convention for repeated indices. Ruppeiner [7,14] notes that the Hessian of the system entropy qualifies as a Riemannian metric and defines this to be the thermodynamic metric to be

$$g_{\alpha\beta} = -\frac{\partial^2 S}{\partial X^\alpha \partial X^\beta}. \tag{7}$$

Ruppeiner's choice for the scale variable X^{sc} is the volume V of the system [11]. In this ensemble, domains correspond to actual spatial regions and this allowed for a more intuitive interpretation of quantities introduced by the Ruppeiner metric. Thus in the literature, this is also the usual choice. We refer to the metric resulting from this choice the Ruppeiner-*V* metric. However, nothing really prohibits choosing alternative scale variables like the number of particles N of the system, which is the particular choice we investigate in this paper. The motivation for this is that in phase transition analysis, N is often chosen to be constant [8,49], as in the ensemble assumed by the Helmholtz and Gibbs free energy. The resulting metric for this choice differs from the usual Ruppeiner-*V* metric, and we refer to it as the Ruppeiner-*N* metric. It is thus worth noting how the metric is seemingly sensitive to the choice of ensemble. While equally valid, the Ruppeiner-*N* metric is an unpopular choice in the literature. Nevertheless, there is at least one study [25] that used this metric. It is the principal

object of this work to show how the Ruppeiner-N metric can work better than its far more popular sibling Ruppeiner-V for geometric constructions of fluid phase diagrams.

Writing Eq. (6) as

$$P_A = C\exp\left[-\frac{1}{2k}g_{A_0}(\delta\mathbf{X}_A,\delta\mathbf{X}_A)\right], \tag{8}$$

$$= C\exp\left(-\frac{1}{2k}|\delta\mathbf{X}_A|^2_{A_0}\right), \tag{9}$$

we see that the probability of the system to fluctuate from its equilibrium state A_0 to a nearby state A is measured by the distance between A and A_0 under the Ruppeiner metric; the smaller the distance, the larger the probability.

Let us now consider the case when A is distant from the equilibrium state A_0. We let the system go through a series of stepwise fluctuations that will bring the system from A_0 to A. The physical picture of this is that we have a series of baths with preset temperatures, pressures, etc. We immerse the system to one bath after another until it reaches the state A. Let the intermediate states be indexed by t from $t=0$ to $t=\tau$. The total probability of going from A_0 to A is then $P_{A_0\to A} = P_{A_0\to A_1}P_{A_1\to A_2}\dots P_{A_{\tau-1}\to A_\tau}$ or

$$P_{A_0\to A} = C\exp\left[-\frac{1}{2k}\int_0^\tau g(\delta\mathbf{X}(t),\delta\mathbf{X}(t))\,dt\right]. \tag{10}$$

Invoking Titu's lemma (a special case of the Cauchy-Schwarz inequality) [50]

$$\frac{1}{N}\left(\sum_{k=1}^N a_k\right)^2 \leqslant \sum_{k=1}^N a_k^2, \tag{11}$$

we find an upper bound of $P_{A_0\to A}$ to be

$$P_{A_0\to A} \leqslant C\exp\left\{-\frac{1}{2k}\left[\int_0^\tau \sqrt{g(\delta\mathbf{X}(t),\delta\mathbf{X}(t))}\,dt\right]^2\right\}. \tag{12}$$

The integral in Eq. (12) is the distance of the path from A_0 to A. We see that the greater the distance, the smaller the upper bound of the probability of the system transitioning from state A_0 to A becomes. In other words, states that are "far" in the thermodynamic space have low transition probabilities. Looking back at Eq. (10), notice that the probability is dependent on the parametrization of states. In finite-time thermodynamics [51], the parameter t is interpreted as time. If the parametrization is such that $g(\delta\mathbf{X}(t),\delta\mathbf{X}(t))$ is constant, we get the equality sign in Eq. (12).

In summary, the Ruppeiner distance gives a measure of the probability of fluctuation from one state to another.

B. Coordinates

We are not constrained to express the Ruppeiner metric using the natural extensive variables of the entropy. Let $Y_\mu := \partial S/\partial X^\mu$ be the conjugate variable of X^μ. Here we use the notation that Greek indices run through all the extensive or intensive variables, while Latin indices exclude the energy $X^0 := E$ and the inverse temperature $Y^0 := 1/T$. From Eq. (7), we can write the Ruppeiner metric as

$$g = -\frac{\partial^2 S}{\partial X^\alpha \partial X^\beta}dX^\alpha dX^\beta, \tag{13}$$

$$= -dX^\mu dY_\mu. \tag{14}$$

With the fundamental relation

$$dE = TdS + P_i dX^i, \tag{15}$$

where P_i is the conjugate of X^i in the energy representation, one can recast Eq. (14) as

$$g = \frac{1}{T}dT\,dS + \frac{1}{T}dX^i dP_i. \tag{16}$$

The Ruppeiner metric is diagonal in the coordinate system (X^k, T), where X^k is the lone extensive variable (aside from the energy and entropy) allowed to vary. In the (N,T) surface where V is constant, we have

$$g_V = \frac{1}{T}\left(-\partial_T^2 F\,dT^2 + \partial_N^2 F\,dN^2\right), \tag{17}$$

where F is the Helmholtz free energy. In the (V,T) surface where N is constant, we have

$$g_N = \frac{1}{T}\left(-\partial_T^2 F\,dT^2 + \partial_V^2 F\,dV^2\right). \tag{18}$$

These can be obtained from Eq. (16) by writing the total differentials dS and dP^i in terms of dT and dX^i.

The two metrics in Eqs. (17) and (18) are different because we are looking at two different surfaces of the same thermodynamic manifold: the hyperplane of constant V (Ruppeiner-V surface) and the hyperplane of constant N (Ruppeiner-N surface). These metrics are induced from the same Ruppeiner metric defined on the whole thermodynamic space. In what follows, we shall refer to Eq. (18) as the Ruppeiner-V metric and Eq. (17) as the Ruppeiner-N metric.

C. Example: van der Waals fluid

The simplest fluid that exhibits phase transitions is the van der Waals fluid [52]. Let us consider its Ruppeiner metric. The ideal van der Waals fluid is characterized by the following pressure and energy EoS [53]:

$$P = \frac{NkT}{V-Nb} - a\frac{N^2}{V^2}, \tag{19}$$

$$E = \frac{3}{2}NkT - a\frac{N^2}{V}. \tag{20}$$

The corresponding Helmholtz free energy is

$$F = -NkT\ln\left[\left(\frac{V}{N}-b\right)(T\eta)^{3/2}\right] - \frac{aN^2}{V}, \tag{21}$$

for some constant η. In our analysis, we always work in the frame (x,T), where x is the number density $x := N/V$. It is also convenient to normalize quantities with respect to their critical values:

$$P_C = \frac{1}{27}\frac{a}{b^2}, \tag{22}$$

$$T_C = \frac{8}{27}\frac{a}{bk}, \tag{23}$$

$$x_C = \frac{1}{3}\frac{1}{b}. \tag{24}$$

From here onward, we will always use normalized quantities where all critical values are set to unity. For example, whenever the temperature "T" appears, we shall take this to mean T/T_C.

Evaluating Eqs. (17) and (18), the Ruppeiner-V and Ruppeiner-N metric of the van der Waals fluid are

$$g_V = \left(\frac{4x}{T^2}\right)dT^2 + \left[\frac{24}{x(x-3)^2} - \frac{6}{T}\right]dx^2, \tag{25}$$

$$g_N = \left(\frac{4}{T^2}\right)dT^2 + \frac{1}{x}\left[\frac{24}{x(x-3)^2} - \frac{6}{T}\right]dx^2, \tag{26}$$

respectively. Note that the two metrics are conformal to each other: $g_N = \frac{1}{x}g_V$. We shall study these geometries extensively in what follows.

III. THERMODYNAMIC GEODESICS

An immediate application of the Ruppeiner-N metric is that its geodesics provide an improved coordinate-invariant partitioning scheme for defining phases in thermodynamic state spaces. But first we discuss some preliminaries.

The length s of a curve γ on a space with metric g_{ab} is given by [54]

$$s = \int_\gamma \sqrt{g_{ab}\dot{\gamma}^a\dot{\gamma}^b}\,dt, \tag{27}$$

where a dot on top a variable indicates taking derivative with respect to the parameter t. Geodesics are the curves that extremize the length s. They satisfy the nonlinear differential equation:

$$\ddot{\gamma}^a + \Gamma^a_{bc}\dot{\gamma}^b\dot{\gamma}^c = 0, \tag{28}$$

where Γ^a_{bc} are the Christoffel symbols [55]. The Christoffel symbols are computed from the metric [56]:

$$\Gamma^\alpha_{\mu\nu} = \tfrac{1}{2}g^{\alpha\beta}(g_{\beta\mu,\nu} + g_{\beta\nu,\mu} - g_{\mu\nu,\beta}). \tag{29}$$

The symbol $g^{\alpha\beta}$ with up-up indices refers to the inverse of the metric $g_{\alpha\beta}$ written with down-down indices. Lowered indices after a comma refers to partial differentiation with respect to the corresponding coordinate: $g_{\beta\mu,\nu} = \partial_\nu g_{\beta\mu}$.

In general relativity, point particles, with or without mass, travel along geodesics of the given space time, a four-dimensional pseudo-Riemannian manifold. In thermodynamic geometry, however, no mechanism constrains systems to evolve exclusively along geodesics. Nevertheless, the significance of these geodesics in thermodynamic geometry has been noted in several papers [7,14,16–18,28].

The geodesics of the Ruppeiner metric, being the curves that minimize the average fluctuations between two states [28], were utilized by Diósi *et al.* [29] in their proposal of a covariant rule for classifying liquid and gas states in the van de Waals state space. This rule provided a means of partitioning the van der Waals state space into its liquid and gas regions, even above the critical point. However, as investigated in this paper, the boundary produced using their scheme was not seen to correspond to any of the already-established thermodynamic lines. We show here that we can overcome this weakness by adopting the Ruppeiner-N metric instead of the usual Ruppeiner-V metric. With the Ruppeiner-N metric, we can generate a geodesic-based boundary that neatly divides the liquid and gas states in the subcritical region and divides the supercritical region the same way as the isotherm Widom line does.

In what follows, we first review the Diósi partitioning based on Ref. [29] before discussing our own modified partitioning of the van der Waals state space using the Ruppeiner-N metric.

A. Diósi partitioning of the van der Waals state space

Just for this subsection, we use the dimensionless variables adopted by Diósi *et al.* for easier comparison. The variables are nondimensionalized but *not* normalized, i.e., Eqs. (22)–(24) but without the coefficients 1/27, 8/27, and 1/3, respectively. These numbers become the critical values of the dimensionless pressure, temperature, and density in this definition, respectively.

The first rule of the Diósi partitioning scheme is this:

> If two states belong to the same phase, then the states must be geodesically connected.

Geodesically connected means there is a geodesic curve that contains the two points. An important remark to this definition is that it is intentionally not a biconditional. Thus, this rule alone is insufficient to judge which states belong to a phase.

The authors then argued the following:

> States geodesically connected to states on the phase boundary, known to be at some phase, also belong to that same phase.

For example, states that are geodesically connected to a state on the liquid part of the phase boundary are liquid themselves. The rationale behind this definition is that we are most sure at the phase boundary that a state is at one specific phase because we can compare it to the other coexisting state and we can see the two behaving differently. So clearly, one must be in a phase that the other is not. These two rules can now assign a phase to a set of mutually geodesically connected (*MG-connected*) states—but an issue arises that weakens the physical significance of the Diósi phase regions. Consider the states on the gas part of the phase boundary. By the authors' definition, these states should all be at the gaseous phase. Thus, we should expect these states to be MG connected themselves, but this is not the case for the van der Waals fluid (see Fig. 1). We will talk more about this in a while.

To locate all points of a particular phase in the Diósi scheme, one could imagine doing the following procedure: (1) locate points at the phase boundary (red curve in Fig. 1; part of it overlaps with the blue and green curves) that are MG connected; (2) for each cluster of MG-connected points, propagate geodesics from each point; and (3) check the points in these geodesics that are MG connected. The phase region then constitutes all these MG-connected points from steps 1 and 3. Of course, several issues are already apparent just from enumerating the steps. For one, we are basically trying to cover a two-dimensional region with one-dimensional curves, which would be impossible. We also do not know whether these regions are simply connected.

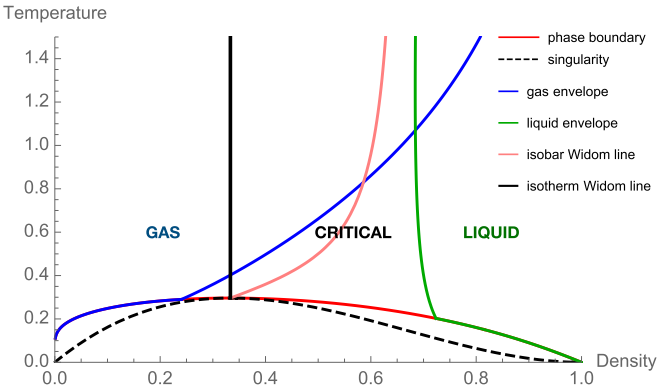

FIG. 1. Diósi partitioning of the van der Waals state space.

To simplify the process, the authors made assumptions so that the boundaries of these regions can be drawn by just looking at the envelope of geodesics emanating from a single sample point at the phase boundary. For example, we go over the gaseous part of the phase boundary ($x < x_C = 1/3$ in Fig. 1). The authors chose to propagate geodesics from an asymptotically low-density gas state ($x = 0.01, T = 0.16$) (see Fig. 2). One can see from the plot that some gaseous states at the phase boundary ($x < 1/3$) are not geodesically connected with the source point, even though these states belong to the same phase in the standard sense. By observation, propagating geodesics at a gaseous source point with a higher density will have an envelope that is farther to the right. Thus, it is the envelope produced from lower densities that bounds the possibly MG-connected gas states. This observation let the authors to consider just a single state at the phase boundary, instead of having to deal with step 1 mentioned from the last paragraph. With the assumption that all the points bounded by this envelope are also MG connected, the region bounded by the phase boundary curve and the "gas" envelope is then taken to be the Diósi gas region. In their study, they made checks on sample pairs of points from a phase region if they are indeed geodesically connected.

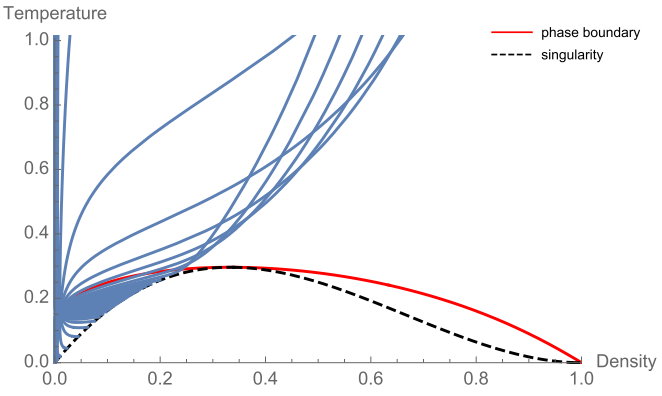

FIG. 2. Geodesics emanating from an asymptotically low-density gas state. One hundred (100) sample geodesics are propagated from the state ($x = 0.01, T = 0.16$). The outer envelope of these curves, excluding states below the phase boundary (metastable states), is the blue curve in Fig. 1.

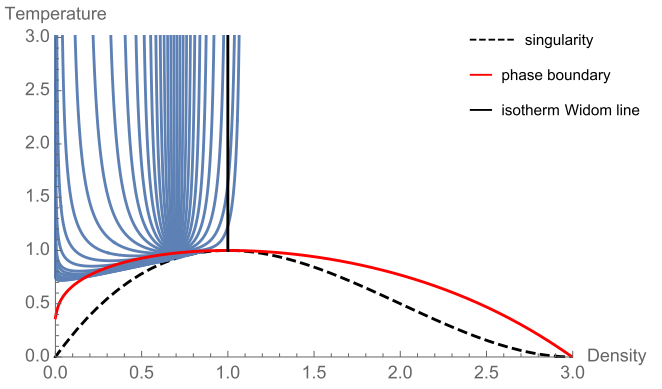

FIG. 3. Geodesics propagating at a gas state on the phase boundary in the Ruppeiner-N van der Waals space. The source point is at ($x = 0.7000, T = 0.9757$). Notice that only a few rays cross the critical isochore, which is also the isotherm thermodynamic Widom line of the van der Waals fluid.

But one question remains: What about the actual gas states, in the standard sense ($x < x_C$, $T < T_C$), that are not included in the Diósi gas region? Easy. They are thrown away into the *critical* region (see Fig. 1), which is just the region whose points are not geodesically connected to all Diósi gas or liquid states. This is one main weakness of the Diósi partitioning scheme; the boundaries it produces do not even completely agree with the phase boundary. In fact, probably the only satisfactory result from the Diósi partitioning is that no two states belonging from two different phases (in the standard sense) are geodesically connected. In short, the Diósi regions and boundaries fail to acquire physical significance.

For the Diósi liquid region, the chosen asymptotically high-density state is ($x = 0.98, T = 0.0196$).

To further test if the Diósi boundaries correspond to possible physical boundaries, we superimposed the isotherm (solid black curve) and isobar (orange curve) thermodynamic Widom line atop the Diósi boundaries (see Fig. 1). A sketch for finding the Widom line of a system is given in Sec. V A. We used Widom lines because these are considered by many authors to be the continuation of the phase boundary on the supercritical region. As can be seen, the Diósi boundaries still ignore the presence of any of these lines.

B. Phase boundaries of van der Waals gas using Ruppeiner-N geodesics

In this subsection, we revert back to the dimensionless and normalized variables in Eqs. (22)–(24).

A general property of geodesics using the Ruppeiner-N metric is that those emanating from gas states ($x < 1$) hardly cross the critical isochore $x = 1$, with the exception of few trajectories. For example in Fig. 3, rays at different initial angles in the (x, T) space are propagated from a single point. The chosen initial point is at ($x = 0.7000, T = 0.9757$), a gas state on the phase boundary. We can see that only a few rays passes the critical isochore with much of them staying at the gas side (to the left of the critical isochore) of the state space. If we lower down the temperature, then fewer rays cross the critical isochore (see Fig. 4). This prompts us

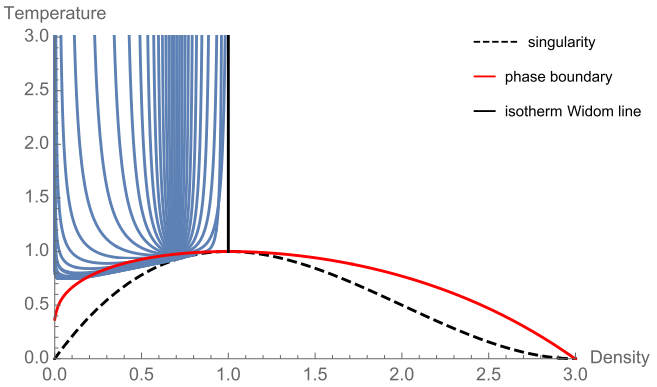

FIG. 4. Geodesics propagating from a gas state slightly below the phase boundary. The source point is at ($x = 0.7000$, $T = 0.9657$), a difference of -0.01 from the temperature value of the source point in Fig. 3. Here rays are no longer seen to intersect the critical isochore or isotherm Widom line.

to check the geodesics emanating from asymptotic states just above the spinodal curve. From Fig. 5, we can see that the geodesics are compressed and bundled along a vertical line (constant x) even though initial angles are varying. Looking at an asymptotic spinodal gas state very near the critical point, we see that no geodesic emanating from this state crosses the critical isochore. That is, all geodesics stay to the left of the critical isochore. The same features hold for the liquid states on the right of the critical isochore. The key observation here is that the geodesics in the Ruppeiner-N space seem to be aware of the presence of the critical isochore. For the van der Waals fluid, the critical isochore turns out to be the isotherm thermodynamic Widom line.

We now state our version of the phase partitioning rule:

> Gas (liquid) states are states that are geodesically connected to any asymptotic spinodal gas (liquid) state.

Our rule generates only one boundary, which is exactly the critical isochore and the isotherm thermodynamic Widom line. Any state on the left of the critical isochore (in Figs. 3–5) is a gas and any state on the right is a liquid. Unlike

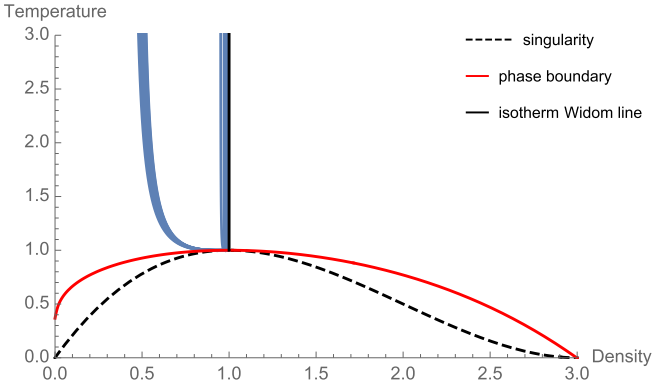

FIG. 5. Geodesics propagating from an asymptotically spinodal gas state very near the critical point. One thousand rays are propagated from the state at ($x = 0.999000$, $T = 0.999999$).

the original Diósi prescription, our partitioning rule separates states in a way that is entirely consistent with the standard definition of gas and liquid states of the van der Waals fluid in the subcritical region. Furthermore, our boundary correctly extends to the supercritical region, where it coincides with the isotherm Widom line. Thus, the phase partitioning rule based on the Ruppeiner-N geodesics gives a more sensible classification van der Waals states throughout the whole state space.

IV. EQUATION OF STATE NEAR THE CRITICAL POINT

Applications of the Ruppeiner metric and the R-crossing method to specific model systems are abundant in the literature [19–21,23–26]. In this paper, we wish to check if the R-crossing method works for general fluids that possess a critical point. We do this by first constructing a general equation of state.

We start with a pressure EoS written as a function of temperature and number density $P(T, x)$ and perform an expansion in the number density about the critical point $x = 1$. The reason for this expansion is because the R-crossing method is expected to work in the neighborhood of the critical point. This is due to Ruppeiner's hypothesis of the Ricci scalar being proportional to the correlation volume near the critical point [19]. Because at the critical point $\partial_x P = \partial_x^2 P = 0$, we keep terms in our expansion up to third order in $(x - 1)$ [57]:

$$P(T, x) = a_0(T) + a_1(T)x + a_1(T)x^2 + a_3(T)x^3. \tag{30}$$

We subject Eq. (30) to a number of constraints that will limit the forms of the a_i functions so that the pressure EoS evolves as expected as the temperature approaches the critical value $T = 1$.

First, we require that below the critical temperature $P(T, x)$ should have two real *extremal* critical points (values of x that extremizes P, not to be confused with the thermodynamic critical point). Let $x_1(T)$ and $x_2(T)$ be the extremal critical points of P at a given temperature. Then, we should have

$$\partial_x P \propto [x - x_1(T)][x - x_2(T)]. \tag{31}$$

At the critical temperature, x_1 and x_2 should coincide at the critical point: $x_1(T = 1) = x_2(T = 1) = 1$. Just above the critical temperature, no extremal critical points should exist because the pressure EoS should now be stable everywhere. So, in general, x_1 and x_2 are complex numbers. We decompose them to their real and imaginary parts,

$$x_1(T) = f_1(T) + i\, g_1(T), \tag{32}$$

$$x_2(T) = f_2(T) + i\, g_2(T). \tag{33}$$

Even though the $x_1(T)$ and $x_2(T)$ are complex-valued functions, we should not see any imaginary numbers in the full form of $P(T, x)$. Integrating Eq. (31) with respect to x and zeroing out all imaginary terms, we get the following

constraints:

$$f_1(T) = f_2(T), \tag{34}$$

$$g_1(T) = -g_2(T). \tag{35}$$

We now write the extremal critical points as

$$x_\pm = f(T) \pm i\,\tilde{g}(T). \tag{36}$$

Now that the behavior of the pressure EoS above the critical point has been worked out, we return to the subcritical region. When $T < 1$, $x_\pm(T)$ should be purely real so that the two extremal critical points exist. If we let $i \cdot \tilde{g}(T) = \sqrt{g(T)}$, where $g(T)$ is a function such that $g(T < 1) \geqslant 0$, $g(T = 1) = 0$, and $g(T > 1) < 0$, then we see that $x_\pm(T)$ acquires the desired properties we have for it: $x_\pm(T < 1) \in \mathbb{R}$, $x_\pm(T = 1) = 1$, and $x_\pm(T > 1) \notin \mathbb{R}$. With this, the final form of our general cubic EoS becomes

$$P = h(T)\left\{\tfrac{1}{3}x^3 - f(T)x^2 + [f^2(T) - g(T)]x + c(T)\right\}. \tag{37}$$

So far, we have four free functions of temperature characterizing a specific system near a critical point. We further impose these constraints to the free functions:

$$P(1, 1) = 1, \tag{38}$$

$$\frac{d}{dT}P(T, x_\pm(T))|_{T=1} > 0, \tag{39}$$

$$\left.\frac{\partial P}{\partial x}\right|_{T>1} > 0. \tag{40}$$

Equation (38) sets the critical value of the dimensionless pressure to unity. Equation (39) ensures that the equation $P = P(T < 1, x)$ will not have multiple roots in x for $P > 1$. This removes the possibility of having coexistent states with pressures greater than the critical value. Finally, Eq. (40) imposes that the system be stable above the critical temperature.

The corresponding Helmholtz free energy is

$$F = h(T)\left\{\frac{1}{6}x^2 - f(T)x + [f^2(T) - g(T)]\ln x - \frac{c(T)}{x}\right\} + j(T). \tag{41}$$

calculated from the relation $P = -(\partial F/\partial V)_T$ [58]. Notice the additional free function $j(T)$.

A. Function parameters

We have a total of five free functions in our expansion, $c(T)$, $f(T)$, $g(T)$, $h(T)$, and $j(T)$, that characterize a fluid system near a critical point. For example, the van der Waals fluid with the pressure [59] and temperature [60] EoS

$$P = \frac{8xT}{3 - x} - 3x^2, \tag{42}$$

$$T = \frac{1}{4}(E + 3x), \tag{43}$$

using normalized variables (E stands for the normalized internal energy) has the following assignment in our parametrized expansion:

$$\begin{aligned} c(T) &= -1/9, \\ f(T) &= 1/3 + 2/(3T), \\ g(T) &= f^2(T) - 1, \\ h(T) &= 9T/2, \\ j(T) &= -4T[\ln(T) + K], \end{aligned} \tag{44}$$

where K is a constant.

Our expansion also works for nonfluid systems, where the order parameter is different from the number density x, after some minor modifications. To illustrate this, we look at the Curie-Weiss ferromagnet which is the mean-field approximation to the Ising model [61]. Its Helmholtz free energy per spin $\mathfrak{F}$ is given by [62]

$$\mathfrak{F} = -kT\left[m\,\mathrm{arctanh}\,m + \frac{1}{2}\ln(1 - m^2) - \frac{1}{2}\frac{T_c}{T}m^2 - \ln 2\right], \tag{45}$$

where T_c is the critical temperature. Equation (37) still holds, although this will now be the expression for the external magnetic field H, and number density x is replaced by the mean magnetization per spin m. Since $H = (\partial\mathfrak{F}/\partial m)_T$, Eq. (41) is replaced with

$$\mathfrak{F} = h(T)\left\{\tfrac{1}{12}x^4 - \tfrac{1}{3}f(T)x^3 + \tfrac{1}{2}[f^2(T) - g(T)]x^2 + c(T)x\right\} + j(T). \tag{46}$$

The corresponding free functions for the Curie-Weiss magnet are

$$\begin{aligned} c(T) &= 0, \\ f(T) &= 0, \\ g(T) &= 1 - T, \\ h(T) &= T, \\ j(T) &= 0, \end{aligned} \tag{47}$$

where we have set $k = 1$ and $T_c = 1$ to normalize and remove the dimensions of the thermodynamic variables.

Finally, we look at some of these free functions and their physical significance. The functions $f(T)$ and $g(T)$ model the spinodal curve of the fluid through

$$x_\pm(T) = f(T) \pm \sqrt{g(T)}, \tag{48}$$

following Eq. (36). Meanwhile, the function $j(T)$ sets the isochoric heat capacity of the system from the relation $C_V = -T(\partial^2 F/\partial T^2)_V$ [63].

V. RICCI CONSTRUCTION OF THE PHASE BOUNDARY AND THE ISOBAR WIDOM LINE

In this section, we discuss the implications of Ruppeiner's hypothesis in Eq. (1) that the Ricci scalar is proportional to the correlation volume near the critical point of a system. As discussed in Sec. I, this introduces an alternative method for computing the phase boundary and the (isobar) Widom line, which we collectively call the *Ricci construction*. For the reader's convenience, a summary of the different methods is

TABLE I. Terminology and definitions of the standard or thermodynamic and Ricci-constructed phase boundary and isobar Widom line.

	Standard construction	Ricci construction
Phase boundary	Maxwell phase boundary (coexistent states have equal Gibbs free energy)	Ricci phase boundary (coexistent states have equal Ricci scalar)
Isobar Widom line	Widom line (maximum isobaric heat capacity along isobars)	Ricci-Widom line (maximum Ricci scalar along isobars)

presented in Table I. We now apply the Ricci construction on the van der Waals fluid and one sample fluid from our EoS class presented in Sec. IV with the following choice of free functions:

$$\begin{aligned} c(T) &= 2/3 - (1-T), \\ f(T) &= 1, \\ g(T) &= 1 - T, \\ h(T) &= 1, \\ j(T) &= -T^2/2. \end{aligned} \tag{49}$$

This is one of the simplest choice of free functions. We simply call this system *Fluid A*. We also looked at two other sample systems (plots not shown): One has instead $g(T) = 1 - T + (1-T)^2$ and one has $f(T) = T$, as compared to the choices made above. The findings, however, are qualitatively the same as with Fluid A's.

We shall also generate the corresponding thermodynamic lines using standard methods from thermodynamics and compare the resulting curves. These methods are discussed in the following subsection.

A. Calculating phase boundaries and the Widom line

1. Standard thermodynamic construction

The phase boundary and the (thermodynamic) Widom line can be readily computed using standard methods in thermodynamics. The standard Maxwell phase boundary is computed by finding pairs of states with different densities, x_A and x_B, for every value of the temperature less than the critical value that satisfies the equality of pressure as dictated by a pressure EoS,

$$P(T, x_A) = P(T, x_B), \tag{50}$$

and the equality of the Gibbs free function (thus, the chemical potential $\mu = G/N$ as well) [64],

$$G(T, P, x_A) = G(T, P, x_B). \tag{51}$$

The two unknowns x_A and x_B are completely determined from Eqs. (50) and (51).

Meanwhile, the isobar thermodynamic Widom line is directly computed by finding the maximum of the isobaric heat capacity at lines of constant pressure. We use the isobar variant of the Widom line as this is the definition most often used in the literature [19,33,35]. Given a pressure EoS $P(T, V, N)$ and a corresponding Helmholtz free energy $F(T, V, N)$, the isobaric heat capacity can be calculated using

$$C_P = -T\left(\frac{\partial^2 F}{\partial T^2}\right)_V - T\left(\frac{\partial P}{\partial T}\right)_V^2 \left(\frac{\partial P}{\partial V}\right)_T^{-1}. \tag{52}$$

2. Ricci construction

The Ricci scalar R is the simplest curvature invariant that can be obtained from two successive contractions of the Riemann tensor $R^\rho_{\sigma\mu\nu}$ [65]

$$R^\rho_{\sigma\mu\nu} = \Gamma^\rho_{\nu\sigma,\mu} - \Gamma^\rho_{\mu\sigma,\nu} + \Gamma^\rho_{\mu\lambda}\Gamma^\lambda_{\nu\sigma} - \Gamma^\rho_{\nu\lambda}\Gamma^\lambda_{\mu\sigma}, \tag{53}$$

$$R_{\sigma\nu} = R^\mu_{\sigma\mu\nu}, \tag{54}$$

$$R = g^{\sigma\nu} R_{\sigma\nu}. \tag{55}$$

For diagonal metrics, which are the ones we will work with, the curvature is given by [66]

$$R = \frac{1}{\sqrt{g}}\left[\frac{\partial}{\partial x^1}\left(\frac{1}{\sqrt{g}}\frac{\partial g_{22}}{\partial x^1}\right) + \frac{\partial}{\partial x^2}\left(\frac{1}{\sqrt{g}}\frac{\partial g_{11}}{\partial x^2}\right)\right]. \tag{56}$$

Widom [47] argued that the correlation length must be equal for coexistent states. And by Eq. (1), the Ricci scalar must also be equal for two coexistent states. Thus, the Ricci phase boundary is computed from Eq. (50) and, this time, from the equality of the Ricci scalars

$$R(T, x_A) = R(T, x_B), \tag{57}$$

in place of Eq. (51).

Equation (1) also implies that near the critical point the isobar (isotherm) statistical Widom line should be calculable from the Ricci scalar. Since the Ricci scalar is proportional to a power of the correlation length in this region, one can locate instead the maximum of the Ricci scalar along isobars (isotherms) instead of the correlation length. That is, we collect the values of the number density x that maximize $R(T(P, x), x)$ for a given pressure P. This collection of points (x, P) is supposed to be the isobar statistical Widom line. We call this Widom line generated using the Ricci scalar the *Ricci-Widom line*. The strength of the Ricci-Widom line is that it appeals to the original statistical definition of the Widom line, i.e., the locus of correlation length maxima. This is in contrast to the thermodynamics-based standard construction of the Widom line. In other words, the standard Widom line computed in this paper is an isobar thermodynamic Widom line and the Ricci-Widom line is an isobar statistical Widom line.

The standard and Ricci-based phase boundary and isobar Widom line for the van der Waals fluid and Fluid A are shown in Figs. 6 and 7. Figure 6 plots the phase boundaries in the P-T plane while Fig. 7 plots the coexistent states and the Widom lines of the sample thermodynamic systems.

B. Equivalence of Maxwell and Ricci phase boundaries

As can be seen in Figs. 6 and 7, the Maxwell and Ricci phase boundaries of the van der Waals and Fluid A all coincide near the critical point. Our plots in Figs. 6 and 7 are qualitatively similar to the calculated Maxwell phase boundary of

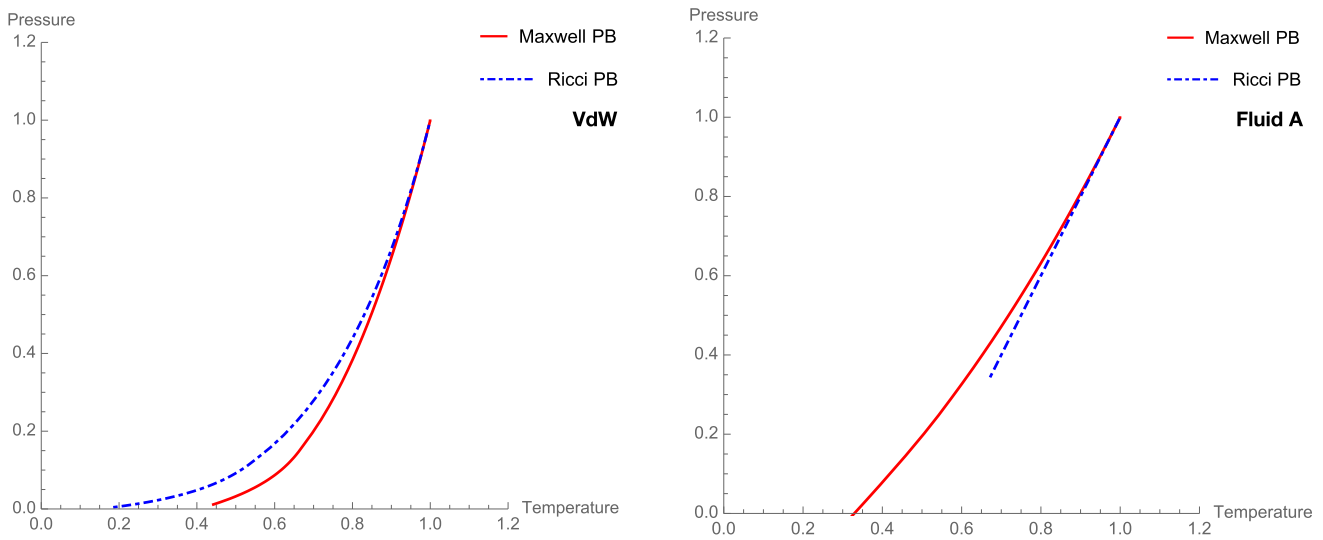

FIG. 6. Maxwell and Ricci phase boundaries of the van der Waals fluid and Fluid A. Normalized thermodynamic variables are used.

other fluid models [23,67]. It seems then that this is a property of a large group of systems, if not universal.

Here we prove that the Maxwell and Ricci phase boundaries are guaranteed to agree near the critical point using the EoS expansion presented in Sec. IV. Figure 8 shows a generic pressure EoS plot at a subcritical temperature in a pressure-density frame. The equation $P = P(T, x)$ has multiple density roots in the interval $[P_{\min}, P_{\max}]$. These roots lie in the interval $[x_{\min}, x_{\max}]$. However, roots in the interval $[x_A, x_B]$ correspond to thermodynamically unstable states. The densities x_A and x_B are the densities of the spinodal gas and liquid states, respectively. Stable multiple roots, then, must lie along the intervals $I_g = [x_{\min}, x_A)$ and $I_l = (x_B, x_{\max}]$. This means that coexistent states (roots that additionally satisfy Eq. (51) for the Maxwell phase boundary states, and (57) for the Ricci phase boundary states) must also be in $I_g \cup I_l$. Coexistent gas states are in I_g and coexistent liquid states are in I_l. Near the critical point where the EoS may be expressed using our expansion in Eq. (37), the measure (length) of both intervals is given by $\sqrt{g(T)}$. However, recall that we demanded this free function to vanish at the critical point so that the pressure EoS may feature a critical point. Thus, as the temperature approaches the critical value, the length of the intervals I_g and I_l approaches zero. These narrowing intervals I_g and I_l squeeze the Maxwell and Ricci phase boundaries together until they meet at the critical point.

Turning to the phase boundary as plotted in the pressure-temperature frame, we can also show that Maxwell and Ricci phase boundaries are tangent to each other at the critical point, as can be seen in Fig. 6. The curve $P_{\min}$ as function of T is given by $P_{\min} = P(T, x_{\min}(T))$, and the curve $P_{\max}$ by $P_{\max} = P(T, x_{\max}(T))$:

$$P_{\min}(T) = \tfrac{1}{3}h(T)[3c(T) - 3f(T)g(T) + f(T)^3 - 2g(T)^{3/2}], \tag{58}$$

$$P_{\max}(T) = \tfrac{1}{3}h(T)[3c(T) - 3f(T)g(T) + f(T)^3 + 2g(T)^{3/2}]. \tag{59}$$

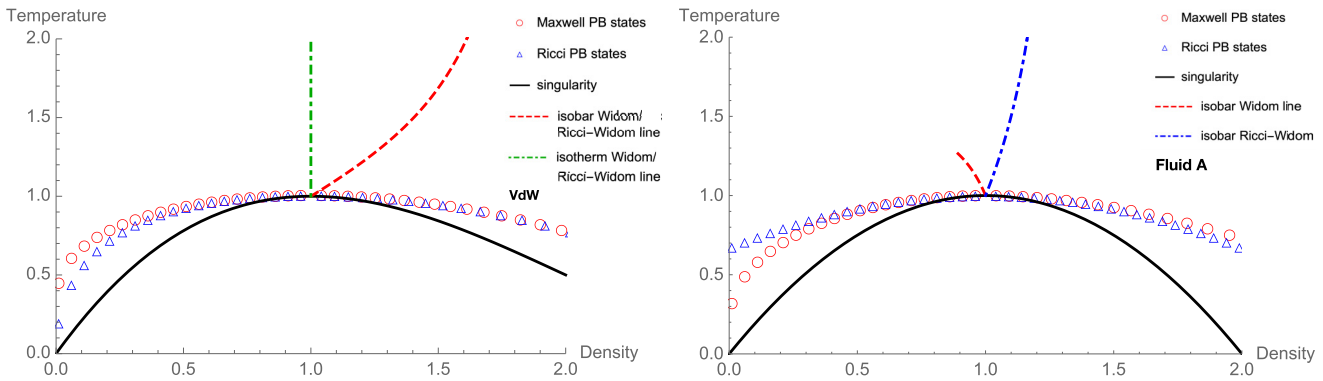

FIG. 7. Maxwell and Ricci phase boundaries of the van der Waals fluid and Fluid A as plotted in a temperature-density frame. Normalized thermodynamic variables are used. The Ricci-Widom line of Fluid A ends not too far from the critical point. Its Ricci curvature no longer have relative maxima at pressures far from the critical value. This is just reasonable since the EoS given for Fluid A is only an expansion around the critical point.

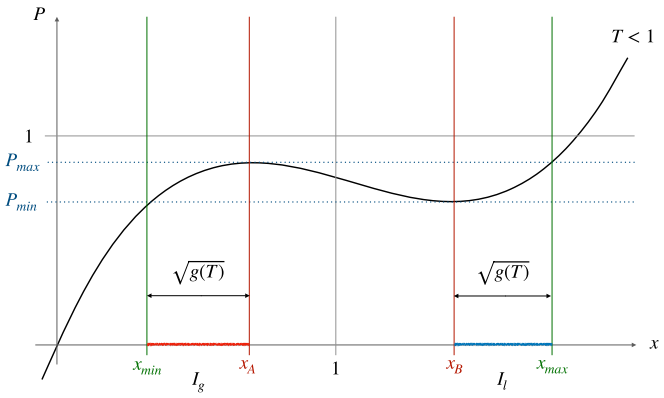

FIG. 8. A pressure EOS at a temperature below and near the critical value.

A sample plot of these curves are shown in Fig. 9. Let $P_M(T)$ and $P_R(T)$ be the Maxwell and Ricci phase boundaries in the P-T plane. As discussed previously, $P_{\max}(T)$ and $P_{\min}(T)$ bounds $P_M(T)$ and $P_R(T)$ from above and below, respectively. We note two things: (1) $P_{\max}(T=1) = P_{\min}(T=1)$, and (2) $P'_{\max}(T=1) = P'_{\min}(T=1)$, since

$$|P'_{\max}(T) - P'_{\min}(T)| = \tfrac{2}{3}\sqrt{g(T)}\,|3h(T)g'(T) + 2g(T)h'(T)| \tag{60}$$

and $g(T=1) = 0$. Because the bounding curves meet at the critical point with the same slope, the Maxwell and Ricci phase boundaries are squeezed together and forced to have equal slopes at the critical point.

Turning for a moment to magnetic systems, this result applies as well to the Curie-Weiss ferromagnet, as we have shown that the Curie-Weiss EoS fits our proposed expansion [68]. This is consistent with the results reported in Ref. [62].

Finally, we note that we did not assume a specific form of $G(T, P, x)$ or $R(T, x)$ in Eqs. (51) and (57) in our analysis. While our analysis supports the Ruppeiner's R-crossing theorem, it also reveals that it is not unique to the Ruppeiner metric that a phase boundary can be generated consistent with the standard curve. In fact, any construction that chooses pairs of coexistent states lying in the interval I_g and I_l will produce a phase boundary that matches the Maxwell phase boundary at the critical point.

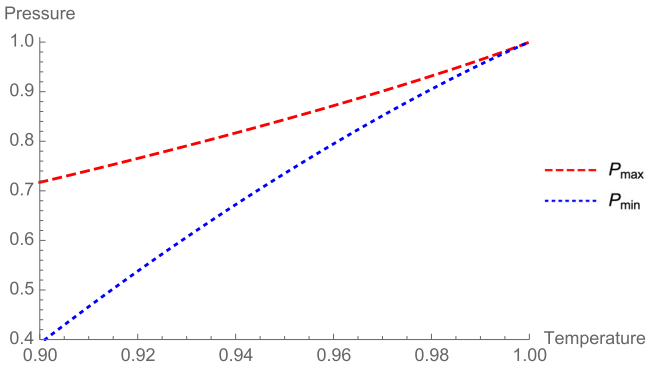

FIG. 9. Bounding curves of the phase boundary on the P-T plane. This sample plot uses the expanded van der Waals EOS in Eq. (44).

C. Equivalence of van der Waals Widom lines and disparity in Fluid A

In contrast to the Maxwell and Ricci phase boundaries, the agreement of the Widom and Ricci-Widom line near the critical point does not necessarily hold for arbitrary EoS. Already with Fluid A, the Widom and Ricci-Widom lines are seen to run on different directions just from the critical point.

While for Fluid A we observed generally poor agreement of the Widom and Ricci-Widom lines, the complete opposite was seen for the van der Waals case. The Widom and Ricci-Widom lines of the van der Waals fluid are exactly the same, for both the isotherm and the isobar variant. The isobaric heat capacity of the van der Waals fluid can be expressed as [69]

$$C_P(P, x) = \frac{4[5P + 3x^2(2x-1)]}{3[P + x^2(2x-3)]}. \tag{61}$$

Meanwhile, the Ricci curvature of the van der Waals fluid (in the Ruppeiner-N metric) is

$$R(T, x) = -\frac{x(x-3)^2[x(x-3)^2 - 8T]}{8[x(x-3)^2 - 4T]^2}. \tag{62}$$

With the pressure EoS of the van der Waals fluid, the temperature in Eq. (62) can be expressed as a function of the pressure and density. What is surprising is that while the two functions are entirely different, their maxima along isobars and isotherms turns out to be exactly coincident, lying at

$$P_{\text{Wid}}(x) = \frac{x^3}{2-x}, \tag{63}$$

and $x = x_C = 1$ for $x \geqslant 1$, respectively. In the work of May and Mausbach [20] where the authors used the usual Ruppeiner-V metric, the Widom and Ricci-Widom lines are only consistent up to their slopes at the critical point, i.e., they are tangent at the point.

It is a curious matter why the Ricci construction of the Widom line works very well for the van der Waals fluid while failing to be consistent with the standard curve for an arbitrary EoS, i.e., an arbitrary choice of free functions. In Ref. [62], it was shown that this disparity is also present in the Curie-Weiss ferromagnet. Aside from the van der Waals fluid, consistent curves are also seen in the Lennard-Jones fluid [20], i.e., the Ricci-Widom line was able to approximate the standard Widom line up to having the same slope at the critical point. The disparity in the curves we found here may be due to the artificial and bare nature of the EoS of Fluid A. We suspect that more realistic equations of state of fluids have certain properties that the EoS of Fluid A and other bare EoS lack. That is, we may need to impose additional physical constraints in our free functions in Eq. (41). Knowing when and how the Ricci-Widom line becomes consistent with the standard Widom line is an important question that we intend to investigate in future works.

VI. CONCLUSION AND RECOMMENDATIONS

This work was an exploration of the geodesics and Ricci curvature of the Ruppeiner geometry of different fluid systems. We have discovered that basing geometric prescriptions for important thermodynamic curves, such as phase boundaries and the Widom line, on an alternative hypersurface of thermodynamic space results in better agreement with standard thermodynamic methods. This alternative hypersurface is one on which the number of particles N is constant as opposed to the usual hypersurface used in applications that keeps the volume V constant. Our overall message is that the induced metric on this constant-N hypersurface, the Ruppeiner-N metric, may be the appropriate metric to use when studying phase diagrams with thermodynamic geometry.

The advantages of the Ruppeiner-N metric already show up in its geodesics. We revisited the pioneering work of Diósi *et al.* [29] that first introduced a geodesic-based redefinition of the phases of the van der Waals fluid using the standard Ruppeiner-V metric. In their classification scheme, however, there is no correspondence between the boundaries they produced and established thermodynamic curves like the phase boundary in the subcritical region and the Widom line in the supercritical region. This disconnect suggests that their partitioning scheme may have little to do with thermodynamics. In contrast, we have shown that geodesics of the Ruppeiner-N metric detect the presence of the isotherm Widom line (locus of isobaric heat capacity maxima along isotherms), which for the van der Waals fluid is also the critical isochore. With our proposed metric, the geodesics select the Widom line as the separating boundary in the supercritical region, thus making thermodynamic geometry more faithful to actual thermodynamics.

Beyond geodesics, we looked at the Ricci curvature of the Ruppeiner-N metric for different fluid systems. We developed a general expansion of equations of state about a critical point in order to accommodate a broad class of fluid systems in our analysis. In comparing the phase boundary and the Widom line generated by the Ricci construction (R-crossing method) to those calculated using standard thermodynamic methods, we found that the phase boundaries are indeed consistent near the critical point. We also provided an explicit proof guaranteeing this agreement for fluids belonging to our EoS family, which unifies the results of May and Mausbach [21] and Jaramillo-Gutiérrez *et al.* [23], and in magnetic systems such as the Curie-Weiss ferromagnet [62]. We showed that magnetic systems can be made to fit our EoS parametrization after some minor modifications.

Finally, we investigated the Ricci construction of the isobar thermodynamic Widom line (locus of isobaric heat capacity maxima along isobars). We found that unlike the phase boundary, the standard and Ricci-based Widom lines do not generally agree for systems belonging to our EoS family. This may be due to missing additional physical constraints that should be incorporated in choosing the free functions of our EoS expansion. It is worth noting that the same disparity of the Widom lines also occurs in the case of the Curie-Weiss ferromagnet [62], even though this is not a fluid system. For more canonical fluid models, like the van der Waals and the Lennard-Jones fluid [20], the Ricci construction of the Widom line is able to approximate the standard thermodynamic curve close to the critical point. For the van der Waals fluid, we showed that the Ricci construction gives the exact same Widom line obtained from standard methods, but this is true only when the Ruppeiner-N metric is used. This is an improvement from the results of May and Mausbach [20] which used the usual Ruppeiner-V metric, in which the Ricci-constructed Widom line is only tangent to the standard curve at the critical point.

Our work opens several directions for future study. We exclusively focused on fluids, so it remains to be investigated what the replacement of the Ruppeiner-V by the Ruppeiner-N metric could bring to nonfluid systems. It is of great interest to check if the advantages we report here can also be observed in other systems. Much of what is known about the Ruppeiner geometry is based on the Ruppeiner-V metric, which is more intuitive and gives a ready interpretation to some quantities that can be computed, but we see no fundamental reason against using the Ruppeiner-N metric. It remains to be seen what other results in the thermodynamic geometry literature will be changed or enhanced by our proposal. In this paper, we have shied away from exploring deeper theoretical and interpretational aspects of the Ruppeiner-N metric, and it remains a mystery why it works better than the traditional Ruppeiner-V metric for the applications we considered.

Finally, further refinements can be made to the fluid EoS expansion we presented. The flexibility of our EoS parametrization is quite wide with its five free functions, whose physical interpretations we left unexplored. It is a curious matter that the Ricci construction of the Widom line should work very well for some systems, but not in general, and our hunch is that this may serve as a guide toward meaningfully restricting the free functions. One may start by turning the question around and asking what conditions the free functions must satisfy for the Ricci construction to generate a Widom line that is consistent with the standard curve. We leave this and related questions to future work.

Data availability. The Mathematica notebooks used to generate plots in this study can be accessed on Github at `krlodeleon/thermo-geom`. The code uses *xAct* packages by J. M. Martin-Garcia *et al.*

[1] J. W. Gibbs, *The Collected Works of J. Willard Gibbs*, Technical Report (Yale University Press, New Haven, CT, 1948).

[2] C. Carathöodory, Untersuchungen über die grundlagen der thermodynamik, Math. Ann. **67**, 355 (1909).

[3] R. Hermann, *Geometry, Physics, and Systems* (M. Dekker, New York, 1973), Vol. 18.

[4] R. Mrugała, Geometrical formulation of equilibrium phenomenological thermodynamics, Rep. Math. Phys. **14**, 419 (1978).

[5] R. Mrugała, Submanifolds in the thermodynamic phase space, Rep. Math. Phys. **21**, 197 (1985).

[6] F. Weinhold, Metric geometry of equilibrium thermodynamics, J. Chem. Phys. **63**, 2479 (1975).

[7] G. Ruppeiner, Thermodynamics: A Riemannian geometric model, Phys. Rev. A **20**, 1608 (1979).

[8] H. B. Callen, *Thermodynamics and an Introduction to Thermostatistics*, 2nd ed. (John Wiley & Sons, New York, 1985), p. 204.

[9] J. W. Gibbs, *The Collected Works of J. Willard Gibbs* (Yale University Press, United States, 1948).

[10] L. Tisza, *Generalized Thermodynamics* (MIT Press, Cambridge, MA, 1966), Vol. 1.

[11] G. Ruppeiner, Riemannian geometry in thermodynamic fluctuation theory, Rev. Mod. Phys. **67**, 605 (1995).

[12] P. Salamon, J. Nulton, and E. Ihrig, On the relation between entropy and energy versions of thermodynamic length, J. Chem. Phys. **80**, 436 (1984).

[13] G. Ruppeiner, New thermodynamic fluctuation theory using path integrals, Phys. Rev. A **27**, 1116 (1983).

[14] G. Ruppeiner, Thermodynamic curvature measures interactions, Am. J. Phys. **78**, 1170 (2010).

[15] G. Ruppeiner, Thermodynamic curvature from the critical point to the triple point, Phys. Rev. E **86**, 021130 (2012).

[16] T. Feldmann, B. Andresen, A. Qi, and P. Salamon, Thermodynamic lengths and intrinsic time scales in molecular relaxation, J. Chem. Phys. **83**, 5849 (1985).

[17] J. Nulton, P. Salamon, B. Andresen, and Q. Anmin, Quasistatic processes as step equilibrations, J. Chem. Phys. **83**, 334 (1985).

[18] P. Salamon, J. D. Nulton, and R. S. Berry, Length in statistical thermodynamics, J. Chem. Phys. **82**, 2433 (1985).

[19] G. Ruppeiner, A. Sahay, T. Sarkar, and G. Sengupta, Thermodynamic geometry, phase transitions, and the Widom line, Phys. Rev. E **86**, 052103 (2012).

[20] H.-O. May and P. Mausbach, Riemannian geometry study of vapor-liquid phase equilibria and supercritical behavior of the Lennard-Jones fluid, Phys. Rev. E **85**, 031201 (2012).

[21] H.-O. May, P. Mausbach, and G. Ruppeiner, Thermodynamic curvature for attractive and repulsive intermolecular forces, Phys. Rev. E **88**, 032123 (2013).

[22] G. Ruppeiner, P. Mausbach, and H.-O. May, Thermodynamic R-diagrams reveal solid-like fluid states, Phys. Lett. A **379**, 646 (2015).

[23] J. Jaramillo-Gutiérrez, J. L. López, and J. Torres-Arenas, R-crossing method applied to fluids interacting through variable range potentials, J. Mol. Liq. **295**, 111625 (2019).

[24] P. Castorina, M. Imbrosciano, and D. Lanteri, Thermodynamic geometry of strongly interacting matter, Phys. Rev. D **98**, 096006 (2018).

[25] S.-W. Wei, Y.-X. Liu, and R. B. Mann, Ruppeiner geometry, phase transitions, and the microstructure of charged ads black holes, Phys. Rev. D **100**, 124033 (2019).

[26] P. Chaturvedi, A. Das, and G. Sengupta, Thermodynamic geometry and phase transitions of dyonic charged ads black holes, Eur. Phys. J. C **77**, 110 (2017).

[27] G. Ruppeiner, Thermodynamic black holes, Entropy **20**, 460 (2018).

[28] L. Diósi, G. Forgács, B. Lukács, and H. L. Frisch, Metricization of thermodynamic-state space and the renormalization group, Phys. Rev. A **29**, 3343 (1984).

[29] L. Diósi, B. Lukács, and A. Rácz, Mapping the Van der Waals state space, J. Chem. Phys. **91**, 3061 (1989).

[30] P. F. McMillan and H. E. Stanley, Going supercritical, Nat. Phys. **6**, 479 (2010).

[31] G. Simeoni, T. Bryk, F. Gorelli, M. Krisch, G. Ruocco, M. Santoro, and T. Scopigno, The widom line as the crossover between liquid-like and gas-like behaviour in supercritical fluids, Nat. Phys. **6**, 503 (2010).

[32] L. Xu, P. Kumar, S. V. Buldyrev, S.-H. Chen, P. H. Poole, F. Sciortino, and H. E. Stanley, Relation between the Widom line and the dynamic crossover in systems with a liquid–liquid phase transition, Proc. Natl. Acad. Sci. USA **102**, 16558 (2005).

[33] D. Banuti, Crossing the Widom-line—Supercritical pseudo-boiling, J. Supercrit. Fluids **98**, 12 (2015).

[34] V. Brazhkin, Y. D. Fomin, A. Lyapin, V. Ryzhov, and E. Tsiok, Widom line for the liquid–gas transition in Lennard-Jones system, J. Phys. Chem. B **115**, 14112 (2011).

[35] A. Lamorgese, W. Ambrosini, and R. Mauri, Widom line prediction by the Soave–Redlich–Kwong and Peng–Robinson equations of state, J. Supercrit. Fluids **133**, 367 (2018).

[36] K. Nishikawa and I. Tanaka, Correlation lengths and density fluctuations in supercritical states of carbon dioxide, Chem. Phys. Lett. **244**, 149 (1995).

[37] F. Gorelli, M. Santoro, T. Scopigno, M. Krisch, and G. Ruocco, Liquidlike Behavior of Supercritical Fluids, Phys. Rev. Lett. **97**, 245702 (2006).

[38] G. Ruppeiner, Application of Riemannian geometry to the thermodynamics of a simple fluctuating magnetic system, Phys. Rev. A **24**, 488 (1981).

[39] G. Ruppeiner and J. Chance, Thermodynamic curvature of a one-dimensional fluid, J. Chem. Phys. **92**, 3700 (1990).

[40] D. Brody and N. Rivier, Geometrical aspects of statistical mechanics, Phys. Rev. E **51**, 1006 (1995).

[41] B. P. Dolan, Geometry and thermodynamic fluctuations of the Ising model on a bethe lattice, Proc. Roy. Soc. Lond. Ser. A: Math. Phys. Eng. Sci. **454**, 2655 (1998).

[42] B. P. Dolan, D. A. Johnston, and R. Kenna, The information geometry of the one-dimensional Potts model, J. Phys. A: Math. Gen. **35**, 9025 (2002).

[43] W. Janke, D. A. Johnston, and R. P. K. C. Malmini, Information geometry of the Ising model on planar random graphs, Phys. Rev. E **66**, 056119 (2002).

[44] W. Janke, D. A. Johnston, and R. Kenna, Information geometry of the spherical model, Phys. Rev. E **67**, 046106 (2003).

[45] D. C. Brody and A. Ritz, Information geometry of finite ising models, J. Geom. Phys. **47**, 207 (2003).

[46] D. A. Johnston, W. Janke, and R. Kenna, Information geometry, one, two, three (and four), Acta Phys. Pol. B **34**, 4923 (2003).

[47] B. Widom, The critical point and scaling theory, Physica **73**, 107 (1974).

[48] L. Landau and E. Lifshitz, *Statistical Physics* (Pergamon Press, Oxford, 1980), p. 333.

[49] H. Gould and J. Tobochnik, *Statistical and Thermal Physics: With Computer Applications* (Princeton University Press, Princeton, NJ, 2010).

[50] A.-L. Cauchy and Cours D'analyse de l'Ecole, Royale Polytechnique. Premiere Partie. Analyse algébrique. (Imprimérie Royale, Paris, 1821).

[51] P. Salamon and R. S. Berry, Thermodynamic Length and Dissipated Availability, Phys. Rev. Lett. **51**, 1127 (1983).
[52] The simpler example of an ideal gas does not have any phase transitions and corresponds to a flat thermodynamic geometry. This has been studied in Ref. [70].
[53] Ref. [8], p. 74.
[54] W. Klingenberg, *A Dourse in Differential Geometry* (Springer Science & Business Media, New York, 2013), Vol. 51, p. 91.
[55] Ref. [54], p. 79.
[56] Ref. [54], p. 61.
[57] This might look like an expansion about $x = 0$ rather than $x = 1$, but the only point is that we take P around $x = 1$ to be at least cubic in x.
[58] Ref. [8], Sec. 5-2.
[59] Ref. [49], p. 371.
[60] Ref. [8], p. 76.
[61] We direct the reader for a detailed study of the Curie-Wiess magnet under the Ruppeiner metric to Ref. [62]. We shall mention later some of their results to compare with our findings on fluids.
[62] A. Dey, P. Roy, and T. Sarkar, Information geometry, phase transitions, and the Widom line: Magnetic and liquid systems, Physica A **392**, 6341 (2013).
[63] P. Kumar, S. Mahapatra, P. Phukon, and T. Sarkar, Geodesics in information geometry: Classical and quantum phase transitions, Phys. Rev. E **86**, 051117 (2012).
[64] Ref. [8], p. 221.
[65] P. A. Szekeres, *Course in Modern Mathematical Physics: Groups, Hilbert Space and Differential Geometry* (Cambridge University Press, 2004).
[66] For example, Ref. [14].
[67] P. Mausbach, H.-O. May, and G. Ruppeiner, Thermodynamic metric geometry of the two-state st2 model for supercooled water, J. Chem. Phys. **151**, 064503 (2019).
[68] Some small details, however, are different from the analysis for fluids. To mention a few, (1) the critical value of m cannot be set to unity because it is at $m = 0$, (2) the value of the external field H (analog of the pressure P for fluids) where there is coexistence of states is frozen at $H = 0$, and (3) due to the previous point, the curves of $H_{\max}$ and $H_{\min}$ will instead meet at $(T = 1, H = 0)$, in contrast to Fig. 9 where the curves meet at $(T = 1, P = 1)$.
[69] Normalized variables are used in Eq. (61). The isobaric heat capacity is nondimensionalized as $C_P \to (\frac{T_C}{P_C V_C})C_P$, as per Eq. (52).
[70] J. D. Nulton and P. Salamon, Geometry of the ideal gas, Phys. Rev. A **31**, 2520 (1985).